Molecular Cell, Vol. 6, 349–360, August, 2000, Copyright ©2000 by Cell Press

RNA Methylation under Heat Shock Control

Hans Bügl,* Eric B. Fauman,†# Bart L. Staker,†‡ Fuzhong Zheng,§ Sidney R. Kushner,§ Mark A. Saper,†‡ James C. A. Bardwell,* and Ursula Jakob*‖
*Department of Biology
†Biophysics Research Division
‡Department of Biological Chemistry
University of Michigan
Ann Arbor, Michigan 48109
§Department of Genetics
University of Georgia
Athens, Georgia 30602

Summary

Structural, biochemical, and genetic techniques were applied to investigate the function of FtsJ, a recently identified heat shock protein. FtsJ is well conserved, from bacteria to humans. The 1.5 Å crystal structure of FtsJ in complex with its cofactor S-adenosylmethionine revealed that FtsJ has a methyltransferase fold. The molecular surface of FtsJ exposes a putative nucleic acid binding groove composed of highly conserved, positively charged residues. Substrate analysis showed that FtsJ methylates 23S rRNA within 50S ribosomal subunits in vitro and in vivo. Null mutations in *ftsJ* show a dramatically altered ribosome profile, a severe growth disadvantage, and a temperature-sensitive phenotype. Our results reveal an unexpected link between the heat shock response and RNA metabolism.

Introduction

Heat shock proteins are well expressed under normal conditions and are overexpressed under stress conditions including elevated temperature, oxidative stress, and viral infections (Becker and Craig, 1994). The majority of heat shock proteins characterized to date act either as molecular chaperones or as proteases (Gross, 1996).

Recently, gene chip technology was employed to systematically investigate the heat shock response in *E. coli* (Richmond et al., 1999). A total of 77 proteins were detected whose mRNA levels showed a greater than 5-fold induction after heat stress. These represent a largely untapped resource of novel heat shock proteins unrelated to previously studied heat shock proteins. To explore their biological function, we are focusing on those heat shock proteins that are strongly induced. Our strategy is to combine three-dimensional structure determination and biochemical analysis of cell function under both normal and stress conditions. The highly conserved nature of these proteins suggests that our results will be applicable to homologs found in a wide variety of species.

The *ftsJ* gene encoding the 209-residue FtsJ protein was originally identified by Ogura and coworkers (1991) and forms part of the *ftsJ-ftsH* operon in *E. coli*. One promoter of this operon is positively regulated by the heat shock transcription factor σ^{32}. Upon heat treatment, *ftsJ* mRNA levels increase by more than 20-fold (Richmond et al., 1999). This makes FtsJ the fifteenth most heat inducible of the 4290 genes in *E. coli* and the third most heat inducible of those without known function. This paper reports the crystal structure of the FtsJ protein at 1.5 Å resolution in complex with its cofactor S-adenosylmethionine (AdoMet). Functional analyses of FtsJ reveal that it is a member of a novel rRNA methyltransferase family.

Results

FtsJ Is a Member of a Universally Conserved Heat Shock Protein Family

Protein sequence comparisons showed that FtsJ homologs are present in a wide variety of species ranging from eubacteria to archaea to eukarya (Figure 1). The *E. coli* FtsJ protein shows 34% identity to its human homologue. The smallest FtsJ homologs are found in eubacteria and archaea where the proteins are ~210 amino acids long. In several eukaryotes, however, up to three different FtsJ paralogs have been identified ranging in size from 310 to over 840 amino acids. These proteins share the FtsJ domain at the N terminus but differ in the length of their C-terminal extension. *Saccharomyces cerevisiae*, for instance, contains three different FtsJ paralogs: YGN6, YBR061cp, and Sbp1. Of the three, YGN6 (320 aa) is most closely related to the bacterial members of the FtsJ family. It is predicted by PSORT to be localized to mitochondria. YBR061cp is the second, smaller FtsJ homologue (340 aa) and clusters in a phylogenetic tree with FtsJ homologs of the animal kingdom. Spb1 is the largest FtsJ paralog with 841 aa.

Motif searches revealed the presence of an S-adenosylmethionine (AdoMet) binding motif in FtsJ. Iterative searches with PSI-BLAST (Altschul et al., 1997) showed limited but significant sequence similarity between FtsJ and a number of methyltransferases. This was in good agreement with earlier protein sequence predictions which suggested that FtsJ is a methyltransferase (Koonin, 1994), and a recent study which showed that the yeast FtsJ homologue Spb1 binds AdoMet in vitro (Pintard et al., 2000).

FtsJ Binds AdoMet as a Cofactor

In order to study FtsJ, we cloned, overexpressed, and purified the 23.3 kDa FtsJ protein from *E. coli* to apparent homogeneity. Analysis of the spectral properties of FtsJ revealed the presence of a tightly bound cofactor with an apparent absorption maximum of 260 nm. Mass spectrometry and gel filtration studies identified this cofactor as AdoMet (data not shown).

FtsJ Has a Methyltransferase Fold

To determine the FtsJ structure, the protein was cocrystallized in the presence of the AdoMet cofactor. Of only

‖To whom correspondence should be addressed (e-mail: ujakob@biology.lsa.umich.edu).
#Present address: Department of Discovery Technologies, Pfizer Global Research & Development, Ann Arbor, Michigan, 48105.

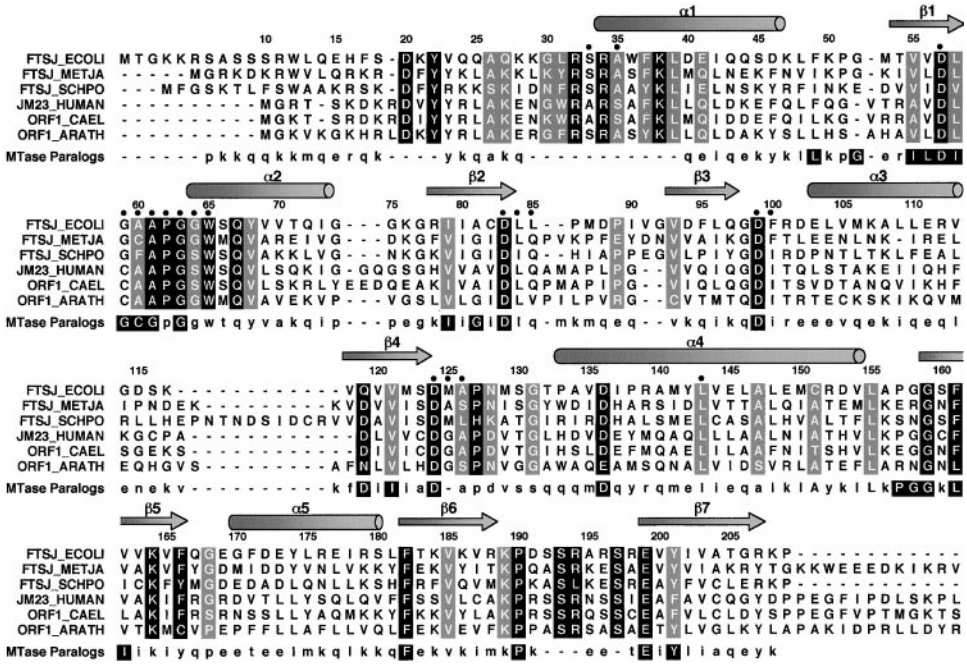

Figure 1. FtsJ Is a Member of a Well-Conserved Heat Shock Protein Family

Twenty-nine sequences considered as FtsJ orthologs were aligned and six representative sequences are shown. FTSJ_ECOLI and FTSJ_METJA are the *E. coli* and *Methanococcus jannaschii* sequences from the SWISSPROT database. FTSJ_SCHPO is an open reading frame from *Schizosaccharomyces pombe* (NCBI GI:2956782) identified in the database as an FtsJ homolog. JM23_HUMAN is the JM23 protein from humans (NCBI CAA06749). ORF1_CAEL is an open reading frame from *Caenorhabditis elegans* (NCBI GI:5824584). ORF1_ARATH is an open reading frame from *Arabidopsis thaliana* (NCBI GI:4539291). This subset, and the orthologs in general, share approximately 33% sequence identity over the aligned positions. Only the portions of the sequences that overlap with FtsJ are shown. The 27 most significantly conserved positions across all orthologs are highlighted in black and the next 26 are highlighted in gray. Residue numbering is for the *E. coli* FtsJ. Filled circles denote residues that contact AdoMet in the crystal structure. The Paralogs line is a consensus sequence derived from the 1112 paralogous sequences as described in Experimental Procedures. The amino acid residue listed is the one with the highest average BLOSUM62 score compared to all residues observed at that position. Paralog positions highlighted in black are the 27 most conserved residues.

four crystals obtained, one diffracted to 1.5 Å resolution and provided a relatively complete native data set to 1.7 Å resolution (Table 1). The structure was phased by isomorphous replacement with derivative data collected from crystals soaked in $HgCl_2$, uranyl acetate, and K_2PtCl_4 solutions. Models for residues 30–209 were refined for both the native (1.7 Å resolution) and mercury (1.5 Å) data sets with R factors of 0.191 (R_{free} = 0.238) and 0.182 (R_{free} = 0.218), respectively. Residues 1–29 were not observed in the electron density maps, and amino-terminal sequencing of the protein confirmed that these residues had been cleaved off during the crystallization.

The FtsJ structure adopts an AdoMet-dependent methyltransferase fold (Fauman et al., 1999) of α/β topology comprised of a seven-stranded β sheet (all parallel except β7) flanked by five α helices (Figure 2). When the FtsJ fold is compared against a nonredundant subset of structures (Dali 2.0; Holm and Sander, 1993), the four most similar proteins are all methyltransferases: catechol-O-methyltransferase (PDB entry 1VID; Vidgren et al., 1994), TaqI polymerase (PDB entry 2ADM; Schluckebier et al., 1997), vaccinia mRNA 2′O-methyltransferase VP39 (PDB entry 1AV6; Hodel et al., 1996), and the rRNA methyltransferase ErmC' (PDB entry 2ERC; Bussiere et al., 1998). Two of these, catechol-O-methyltransferase and VP39, are single domain structures like FtsJ. The catechol O-methyltransferase is similar in size to FtsJ and superposes with an rmsd of 1.97 Å for 109 C_α atoms judged structurally equivalent by LSQMAN (Kleywegt, 1997). VP39 contains a core domain that is homologous to FtsJ (rmsd = 1.73 Å for 109 C_α atoms) but also contains an ~100 residue domain at the carboxyl end that folds over the surface of the core domain. The helix found between β2 and β3 in catechol O-methyltransferase is replaced by a nonhelical crossover in both FtsJ and VP39. The α4 helices in FtsJ and VP39 are uniquely longer (seven and six turns, respectively), compared with the four turns observed in the catechol O-methyltransferase. This helix forms a prominent "tower" adjacent to the AdoMet binding site in both FtsJ and VP39. The interface between this helix and β4 of the sheet in FtsJ is made up of residues specifically conserved among the FtsJ orthologs: Pro-127, Asn-128, Gly-131, Asp-136, Ala-147, Leu-155, Phe-161, and Phe-182.

FtsJ Binds AdoMet with Conserved Residues

Many of the highly conserved residues found in the 29 putative FtsJ orthologs directly contact the AdoMet (Figures 1 and 3). These include the side chains of Ala-35, Pro-62, Trp-65, Asp-83, Leu-84, Asp-99, Asp-124, Met-125, Ala-126, and Leu-143 (Figure 3). The side chains of Ser-33 and Asp-57 indirectly coordinate the AdoMet via well-ordered water molecules. Other contacts to the AdoMet come from the main-chain atoms of conserved

Table 1. Data Collection and Phasing Statistics

Crystal	Resolution (Å)	Number of Reflections		R_{sym}[a] (%)	$<I/\sigma_I>$	Completeness (%)	Phasing Resolution (Å)	R_{cullis}[b]	R_{cullis} anom[c]	PP[d]	Number of Sites
		Observed	Unique								
Native	1.7	124,235	17,520	5.2 (20.0)	15 (8)	87.1 (87)	—	—	—	—	—
$HgCl_2$	1.50	246,794	28,048	6.3 (13.6)	14 (9)	95.1 (93)	1.5	0.66	0.84	1.93	2 Hg
UO_2Ac	1.95	95,294	11,041	14.2 (36.2)	12 (5)	81.9 (80)	3.0	0.81	0.90	1.19	1 Ur
K_2PtCl_4	1.72	158,870	18,575	6.9 (32.6)	20 (6)	96.8 (99)	3.0	0.76	0.90	1.34	2 Pt

[a] $R_{sym} = \Sigma|I_j - <I_j>|/\Sigma I_j$, where $<I_j>$ is the average intensity of reflection j for its symmetry equivalents, including Bijvoet pairs; values in parentheses were calculated from the 5% of data in the highest resolution shell.
[b] $R_{cullis} = \Sigma||F_{PH}| - |F_P + F_H||/\Sigma F_H$, where F_{PH} and F_P are the measured derivative and native structure factor and F_H is the calculated heavy atom structure factor.
[c] R_{cullis} anom $= \Sigma||F_{PH+} - F_{PH-}| - |2\ F_H \sin(\alpha_P)||\ /\ \Sigma\ |F_{PH+} - F_{PH-}|$, where $|F_{PH+} - F_{PH-}|$ is the measured anomolous difference, and α_P is the calculated protein phase.
[d] Phasing power $= <F_H>/E$, where $<F_H>$ is the root-mean-square heavy atom structure factor, and E is the residual lack of closure error.

and nonconserved residues, including Gly-59, Ala-60, Ala-61, Gly-63, Gly-64, and Phe-100. Many of these residues are also conserved in the group of methyltransferase paralogs (Figure 1). When the mRNA methyltransferase VP39 is superimposed on FtsJ, a *cis*-proline near the AdoMet binding site superposes with Pro-62 of FtsJ, also in the *cis*-peptide configuration. It was previously noted that *cis*-proline at this position was a unique feature of the VP39 family of enzymes (Djordjevic and Stock, 1997).

Conserved Residues Form a Groove on the Surface of FtsJ

Adjacent to the reactive C_ε methyl group of AdoMet is a large depression or groove formed by side chains from the central β sheet and the inner surface of $\alpha1$ and $\alpha2$ (Figure 4A). This could represent the substrate binding site in FtsJ. The groove contains a number of conserved and solvent-accessible residues including Arg-34, Ala-35, Lys-38, Ala-126, Lys-164, Phe-166, Arg-194, Ser-197, and Glu-199 (Figures 4C and 4D). The groove also contains a hydrophobic pocket that is adjacent to the extended $\alpha4$ helix and surrounded by residues Met-129, Ile-137, and Phe-166. The lower "wall" of the groove is formed from the positively charged residues Arg-34, Arg-194, and Arg-196. These, together with the adjacent residues Lys-38 and Lys-164, form a prominent electropositive surface in the groove (Figures 4A and 4D). It is noteworthy that nearly all of these positively charged amino acids are specifically conserved within the FtsJ orthologs and are absent in the paralogs (Figure 1).

Substrate Binding Groove of FtsJ Is Reminiscent of VP39

Comparison of the putative substrate recognition surface in FtsJ (Figure 4A) to that of the other closely related methyltransferases revealed striking similarity to the mRNA binding site of VP39 (Figure 4B). VP39 is a multifunctional AdoMet-dependent enzyme in vaccinia virus that methylates the first transcribed nucleotide in mRNA following the 5′ m^7Gppp cap to create a 2′O methyl group. The structure of VP39 in complex with 5′ m^7G-capped, single-stranded RNA hexamer and the competitor S-adenosylhomocysteine (AdoHCys) shows how the RNA molecule binds in this groove on VP39 and positions a nucleoside for the methyl transfer (Hodel et al., 1998). The VP39 mRNA binding groove has significant similarities with the putative substrate binding region of FtsJ both in terms of size and distribution of positively charged residues (Figures 4A and 4B). Modeling studies showed that VP39's RNA substrate fits into FtsJ's putative substrate binding groove and positions a nucleoside next to the reactive C_ε group of AdoMet (data not shown). Moreover, a structure-based sequence alignment of VP39 and FtsJ revealed at least 18 identical residues (data not shown). Of the six VP39 side chains which make direct interactions with the mRNA sugar-phosphate backbone, four have identical counterparts in FtsJ (VP39 residues in italics): *Lys-41* and Lys-38, *Lys-175* and Lys-164, *Ser-205* and Ser-197, *Glu-207* and Glu-199. Of these, only Glu-199 is also conserved in the larger set of methyltransferase paralogs (Figure 1). It is noteworthy that analysis of the substrate binding site in catechol O-methyltransferase, the second most closely related structure to FtsJ, revealed a size and electrostatic surface completely different from FtsJ and VP39.

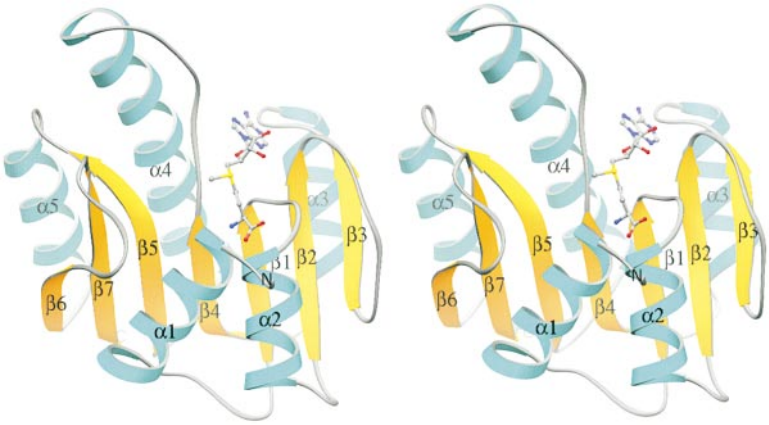

Figure 2. FtsJ Has a Methyltransferase Fold

Stereo diagram of the FtsJ tertiary fold highlighting secondary structure elements. Secondary structures were assigned and the figure was rendered by RIBBONS (Carson, 1997). The bound AdoMet is shown in ball and stick representation.

Two features may reflect specificity differences between the two enzymes. Both VP39 and FtsJ have a "tower" to the left of AdoMet and above the substrate binding groove formed by β4 and the extended α4 helix (Figures 4A and 4B). In VP39, this surface is basic and makes contacts primarily via *Arg-177* to the RNA backbone. In FtsJ, the equivalent residue is Phe-166, and it contributes to a nonpolar nature of the "tower". FtsJ's basic surface is on the lower side of the groove where the guanidinium groups from Arg-194 and Arg-196 may provide a similar ability to hydrogen bond to a nucleic acid substrate (Figures 4A and 4D). Second, VP39 has a narrow opening at the left end of the groove that positions tyrosine and phenylalanine side chains to specifically stack with the methylated base of the 5′ capped substrate. Although FtsJ has a similar sized opening from the groove, it lacks the tyrosine and phenylalanine side chains.

The observations noted above regarding the size and shape of the substrate binding groove, the similarity with VP39, and the conserved location of side chains poised to ligate negatively charged substrates such as RNA are all consistent with the hypothesis that FtsJ might be a nucleic acid binding methyltransferase.

FtsJ Is an RNA-Specific Methyltransferase

To obtain clues as to the cellular function of FtsJ, we explored the potential substrate specificity of the methyltransferase reaction. Various RNA transcripts and DNA were tested in vitro as methyl acceptors. To exclude false negative results due to prior methylation in vivo, a number of substrate RNAs were purified from in vitro transcription reactions. Plasmid DNA was generated from the *ftsJΔ567* deletion strain HB30 (Table 2). Of the in vitro transcribed nucleic acids tested, tRNA showed the highest methyl incorporation when incubated with FtsJ (Figure 5A). Neither mRNA, 16S rRNA, nor DNA showed detectable methyl incorporation (Figure 5A, data not shown). A small but significant amount of methyl incorporation was observed when in vitro transcribed 23S rRNA was tested as a substrate (Figure 5A). To determine the in vivo methylation target of FtsJ, both bulk tRNA and 23S rRNA from wild-type and *ftsJ* deletion strains were prepared, digested into the nucleosides, and analyzed using reverse-phase HPLC chromatography. We detected no unambiguous difference in the elution profiles of tRNA nucleosides prepared from wild-type and *ftsJ* deletion strains. Since only certain tRNAs serve as substrates for FtsJ in vitro (data not shown), we are currently investigating which individual isoacceptor tRNA species, if any, serve as efficient methyl acceptors for FtsJ in vivo. 23S rRNA isolated from the *ftsJ* deletion strain, on the other hand, showed a clear decrease in the level of 2′O-methyluridine (F. Qiu and J. McCloskey, personal communication), suggesting that FtsJ is responsible for methylating 23S rRNA in vivo. This conclusion agrees with studies performed by Caldas et al. (2000), who very recently presented evidence that purified FtsJ methylates 23S rRNA in isolated 50S ribosomal subunits in vitro to create a 2′O-methyluridine at position 2552. It also confirmed our structural analysis that revealed a high structural similarity of FtsJ to the 2′-O-methyltransferase VP39.

23S rRNA modifications are generally known to occur early in the maturation of 23S rRNA (Björk, 1996), yet in vitro methylation of in vitro transcribed, naked 23S rRNA with FtsJ was very inefficient (Figure 5A). The incorporation rate into 23S rRNA, however, improved substantially when ribosomal subunits were used as substrates of FtsJ. As shown in Figure 5B, 50S ribosomal subunits prepared from the *ftsJ* deletion strain showed substantial methyl incorporation. The incorporation of 0.06–0.1 pmol methyl groups/pmol subunit/hr was significantly faster and at least 5 times more efficient than the methyl transfer reaction observed using in vitro transcribed tRNA as substrate. The total methyl incorporation increased to as much as 0.42 pmol methyl groups/pmol 50S subunits when only intact, mature 50S ribosomal subunits were used as substrate (Figure 7B; see below). Negligible methyl incorporation was observed into 50S subunits isolated from the wild-type strain HB24, indicating that in vivo methylation of 23S rRNA by FtsJ goes to near completion (Figure 5B).

FtsJ Is Important for Cell Growth

To determine the role of FtsJ's methyltransferase activity in vivo, an in-frame deletion *ftsJΔ567* was constructed. The deletion of *ftsJ* led to a severe growth defect in *E. coli* under all temperature and growth conditions tested. The *ftsJΔ567* deletion mutant failed to form single colonies on plates after 24 hr of growth (Figure 6). In liquid media, the *ftsJ* deletion strain grew at least 4-fold more slowly than the isogenic wild-type (WT) strain when grown over a wide range of temperatures. These results strongly suggested that FtsJ plays a vital role under normal growth temperatures. The fact that a

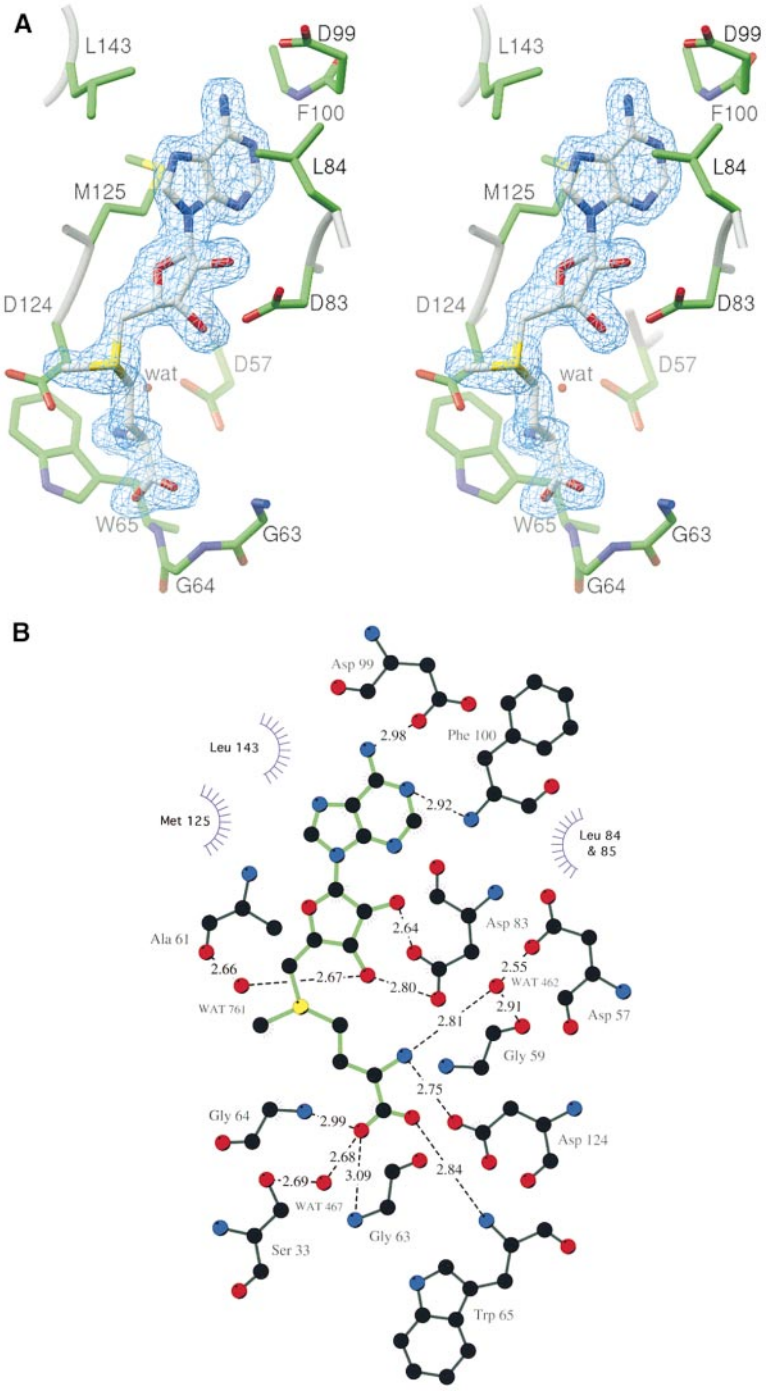

Figure 3. AdoMet Binding Interactions in FtsJ

(A) Stereo diagram of the AdoMet binding site in FtsJ. In light blue are the 2σ contours of F_o–F_c difference map (1.7 Å native data) omitting AdoMet from the calculated structure factors. AdoMet and FtsJ contact residues are shown in ball and stick representation. Green, carbon (FtsJ); gray, carbon (AdoMet); blue, nitrogen; yellow, sulfur; red, oxygen. Figure drawn with RIBBONS.

(B) Schematic diagram showing hydrogen bonds and nonpolar contacts between FtsJ and the AdoMet cofactor (green bonds). Black, carbon; blue, nitrogen; yellow, sulfur; red, oxygen; purple, nonpolar contacts. Figure drawn with LIGPLOT (Wallace et al., 1995).

plasmid just containing the *ftsJ* open reading frame was capable of complementing the growth defect of *ftsJΔ567* deletion strains showed that the observed phenotype was the direct effect of the *ftsJ* deletion and was not due to polarity on downstream genes (Figure 6).

Null mutants in a number of other heat shock proteins such as DnaK, DnaJ, and HtpG have a decreased maximal growth temperature, suggesting that their function becomes essential at high temperatures (reviewed by Gross, 1996). *ftsJ*Δ567 deletion strains show a similar temperature-sensitive phenotype. The maximum growth temperature of the *ftsJ* deletion strains decreased by more than 2°C when compared to an isogenic WT strain on temperature gradient plates. Moreover, while wild-type *E. coli* cells responded to heat shock temperatures (43°C) with an immediate increase in growth rate, *ftsJ*Δ567 deletion strains failed to adjust their growth rate for more than 90 min after exposure to heat shock temperatures. These experiments suggested that FtsJ mediates an important growth-determining step in *E. coli*, which is also essential for the fast adaptation to temperature shifts. In this way, it is similar to many other heat shock proteins that play important roles both before and after heat shock.

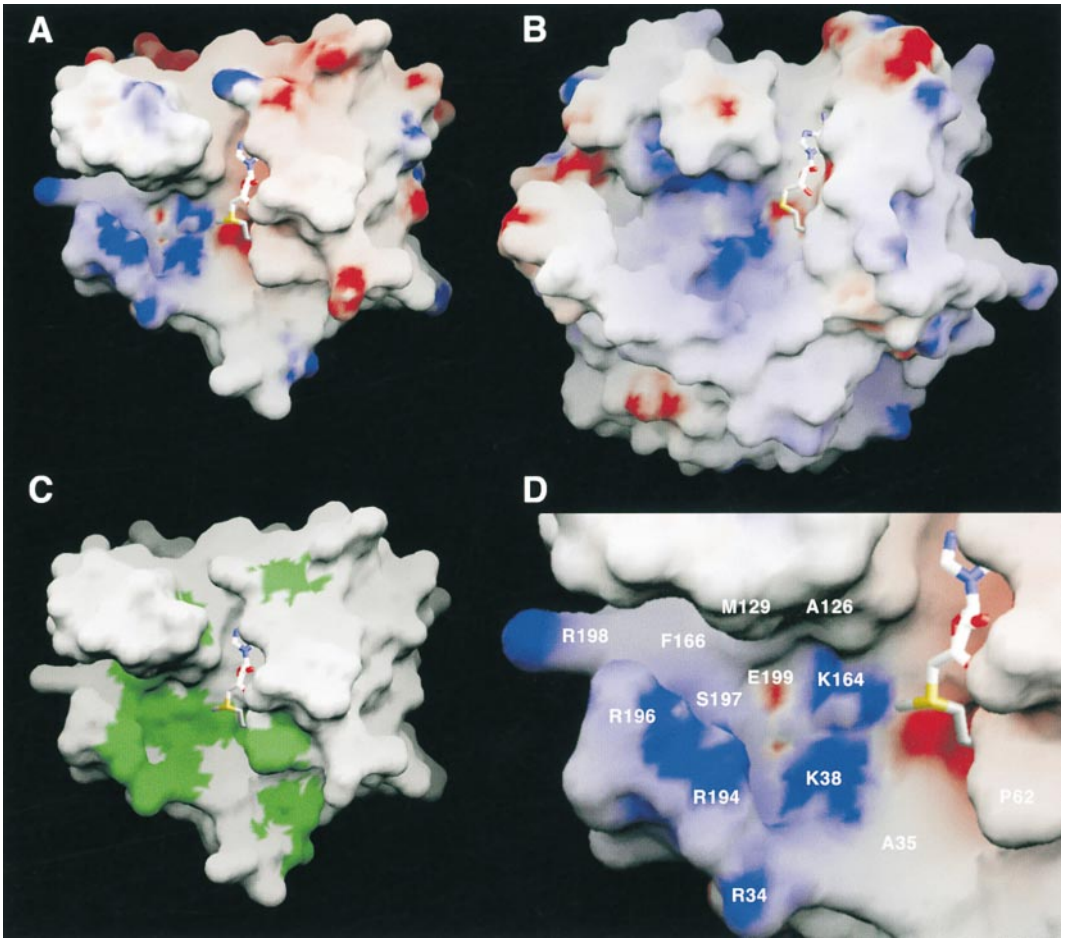

Figure 4. Comparison of FtsJ and VP39 Surfaces

(A) Solvent contact surface of FtsJ colored by electrostatic potential. Potential values range from –15 (blue) to 0 (white) to +15 K_bT (red) where K_b is the Boltzman constant and T is temperature. The bound AdoMet is shown in stick representation. Figures rendered with GRASP (Nichols et al., 1991).

(B) Solvent contact surface of the VP39 mRNA methyl transferase colored by electrostatic potential. The bound AdoHCys is shown. Orientation, scale, and coloring is identical to FtsJ in (A).

(C) Same as (A), but green surfaces highlight side chain atoms of the 27 most conserved FtsJ residues as depicted in Figure 1.

(D) Close-up of putative substrate recognition groove of FtsJ showing many of the residues mentioned in the text.

FtsJ Is Not Involved in Cell Division

FtsJ did not appear to be involved in cell division as originally postulated by Ogura and coworkers (1991) since under all growth conditions tested, the cell morphology of the *ftsJΔ567* mutant was very similar to the WT control. Their observation of an *fts* (filamentous temperature sensitive) phenotype in their *ftsJ*-deletion strains could not be reproduced by us and may have been due to polarity of the kanamycin resistance insertion mutation constructed by Ogura et al. on the downstream *ftsH* gene. Our mutation was an in-frame deletion designed to minimize polarity effects.

ftsJ Deletion Strains Show a Severe Ribosome Defect

To evaluate the role of FtsJ's methyltransfer reaction in the cell, polysome profiles of *ftsJ* deletion strain HB23 and the wild-type strain HB24 were analyzed. This analysis revealed a major ribosome defect in *ftsJ* deletion strains. Under nonstringent magnesium concentrations (10 mM), conditions that stabilize both loosely and tightly associated 70S ribosomes, the wild-type strain HB24 showed a typical polysome profile (Figure 7A). Minor amounts of 50S and 30S ribosomal subunits, major amounts of intact 70S ribosomes, and messenger RNA harboring 2×, 3×, and multiple ribosomes bound were detected. Strains deleted for *ftsJ*, on the other hand, showed a dramatically altered ribosome profile (Figure 7A). They show a substantial increase in the amount of unassembled 30S and 50S subunits, a significant decrease in intact 70S ribosomes, and only trace quantities of actively translating messenger RNA with multiple ribosomes bound. Deletion of the methyltransferase FtsJ causes a very severe ribosome assembly or stability defect that could explain the severe growth defect of *ftsJ* mutant strains. Under stringent magnesium conditions (1 mM) where 70S ribosomes are known to dissociate into 30S and 50S ribosomal subunits, ~40S (I) particles accumulated in the polysome profile of the *ftsJ* deletion strains in expense of mature 50S ribosomal subunits. Hybridization experiments of the respective fractions of the polysome profiles with DNA probes for

Table 2. Strains and Plasmids Used in This Study

Strains	Genotype	Source of Reference
MG1693	*thyA*715, *rph-1*	This study
SK8830	*thyA*715, *zgi-203*::Tn*10*, Tc^R, *ftsJΔ567*, *rph-1*	This study
MG1655	*rph-1*	Lab collection
BL21(DE3)	F^- ompT $hsdS_B(r_B^- m_B^-)$ gal dcm(DE3)	Novagen
HB1	BL21(DE3), pHB1	This study
HB23	MG1655, *zgi-203*::Tn*10*, TC^R, *ftsJΔ567*	MG1655 × P1 (SK8830); This study
HB24	MG1655, *zgi-203*::Tn*10*, Tc^R	MG1655 × P1 (SK8830); This study
HB25	HB23, pHB1	This study
HB30	HB23, pTHZ25	This study
Plasmids	**Relevant Features**	**Source of Reference**
pET11a	T7 expression vector	Novagen
pHB1	pET11a/*ftsJ*	This study
pTHZ25	pet11a/*hslR*	Lab collection

23S rRNA and 16S rRNA revealed that these ~40S ribosomal particles are derived from 50S ribosomal subunits, harboring predominately 23S rRNA. This clearly showed that 50S ribosomal subunits in *ftsJ* deletion strains have severely altered properties, suggesting that the FtsJ-mediated methylation of 23S rRNA in 50S ribosomal subunits plays an important role in the assembly and/or stability of 50S ribosomal subunits in the cells.

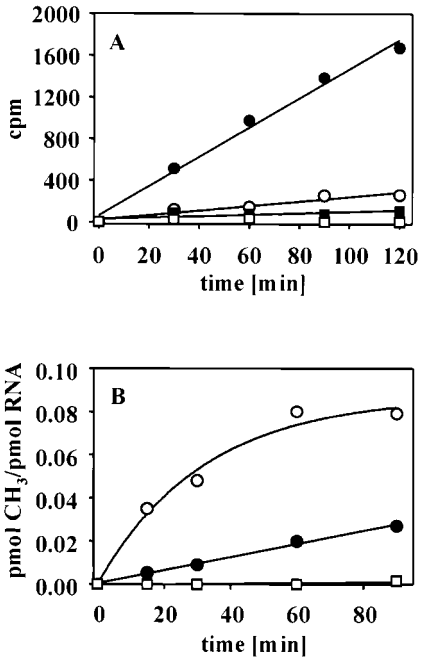

Figure 5. FtsJ Functions as an RNA Methyltransferase In Vitro

(A) FtsJ methylates tRNA in vitro. FtsJ (0.5 μM) was incubated with 2 μM of in vitro transcribed and purified (shaded circles) *B. subtilis* $tRNA^{Asp}$, (open circles) 23S rRNA, (shaded squares) 16S rRNA, or (open squares) 0.3 μM pET11a/*hslR* DNA, respectively. Similar results were obtained when in vitro transcribed *E. coli* $tRNA^{Asp}$ was used.

(B) FtsJ methylates 23S rRNA in 50S ribosomal subunits. FtsJ (0.5 μM) was incubated with 2 μM of 50S ribosomal subunits prepared from (open circles) HB23 (*ftsJΔ567*) and (open squares) HB 24 (WT) or with 2 μM *B. subtilis* $tRNA^{Asp}$ (shaded circles), respectively, in the presence of 50 μM AdoMet (80 μCi/ml) at 37°C. After the time points indicated, aliquots were taken and the methyl incorporation was determined.

FtsJ Effectively Methylates 23S rRNA in Mature 50S Subunits

In order to investigate whether the different ribosomal particles vary in their ability to serve as methyl acceptor for FtsJ, individual fractions of a sucrose gradient were tested in in vitro methylation assays. In the absence of RNase inhibitors, significant degradation of 23S rRNA was observed in *ftsJ* deletion strains. Thus, lysates were treated with the RNase inhibitor RNaseIn (Promega) immediately after cell lysis and prior to the gradient runs. The magnesium and salt conditions chosen for the gradients allowed the separation of 30S from the ~40S particle and from the fully assembled 50S ribosomal subunits as confirmed by dot blot hybridization experiments with 16S and 23S DNA probes (Figure 7B). Under these conditions, no significant degradation pattern occurred in 23S rRNA prepared from ~40S particles or 50S subunits (data not shown). As shown in Figure 7B, the highest methyl incorporation was observed when the mature 50S ribosomal subunit was tested as in vitro substrate. The incorporation rate was at least 4-fold higher than the methyl incorporation into ~40S ribosomal particles.

FtsJ was unable to significantly methylate naked 23S rRNA or 23S rRNA in ~40S ribosomal particles that accumulated under low magnesium conditions but does efficiently methylate 23S rRNA in mature 50S subunits.

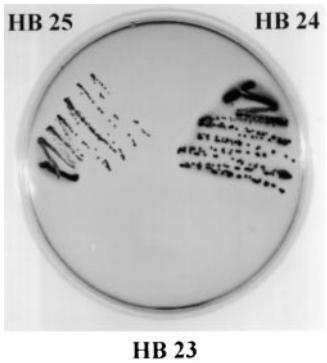

Figure 6. *ftsJ* Deletion Strains Have a Severe Growth Defect

Growth of *E. coli* strains HB24 (WT), HB23 (*ftsJΔ567*), and HB25 (HB23 harboring the FtsJ expression plasmid pHB1) on McConkey plates after 24 hr at 30°C. Similar results were obtained when strains were grown at 37°C and 43°C.

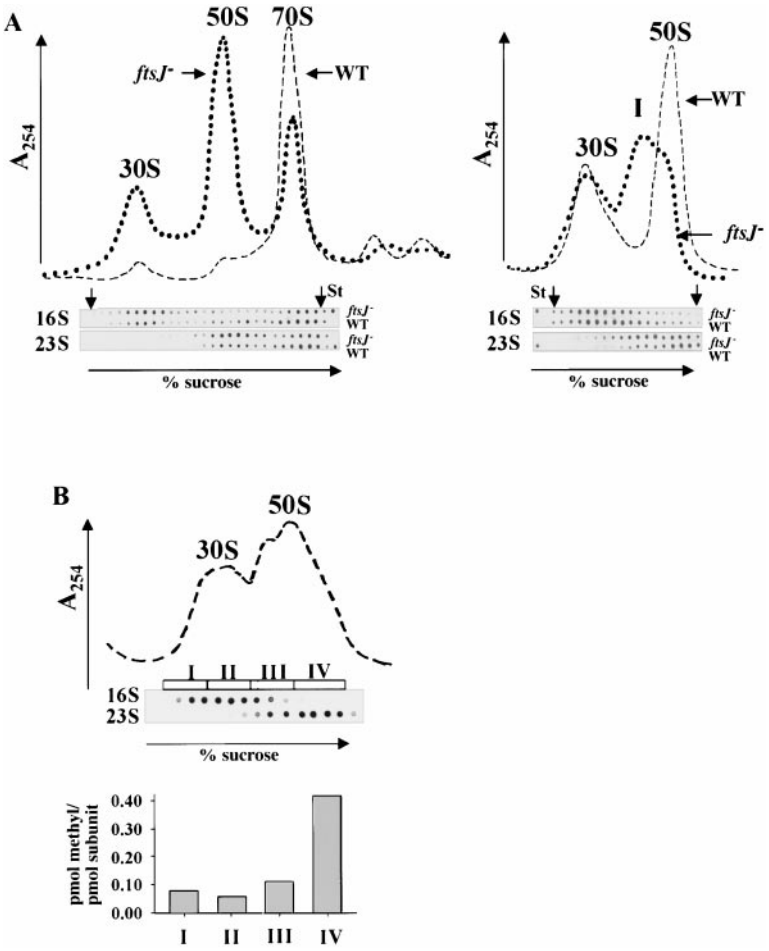

Figure 7. *ftsJ* Deletion Strains Show a Ribosome Defect

(A) Polysome profile of HB23 (*ftsJΔ567*) and HB24 (WT) under (left panel) non stringent salt conditions (10 mM $MgCl_2$, 100 mM NH_4Cl) and (right panel) stringent salt conditions (1 mM $MgCl_2$, 200 mM NH_4Cl) in 10%–50% sucrose gradients. Each fraction of the polysome profile was analyzed for the presence of 16S and 23S rRNA using dot blot analysis. Vertical arrows show the alignment between the profile and the dot blot. St indicates purified 23S rRNA and 16S rRNA used as a standard.

(B) FtsJ methylates 23S rRNA in mature 50S ribosomal subunits. Ribosomes isolated from HB23 (*ftsJΔ567*) were RNaseIn treated and fractionated in a 5%–25% sucrose gradient under stringent salt conditions (1 mM $MgCl_2$, 200 mM NH_4Cl). Fractions were pooled according to rRNA distribution as judged by dot blot analysis of the individual fractions. Four separate pools (2 μM each) corresponding to early 30S fractions (pool I), late 30S fractions (pool II), 40S intermediate fractions (pool III), and late 50S fractions (pool IV) were methylated in vitro using 0.1 μM FtsJ and 8 μM ^{3}H-AdoMet. Mature 50S subunits are most effectively methylated.

This suggested that FtsJ requires 23S rRNA to be correctly folded for an effective methyltransfer reaction.

Discussion

Beyond the Chaperone/Protease Paradigm

The majority of heat shock proteins characterized function either as molecular chaperones or as proteases (Gross, 1996). However, the recent discovery and functional analysis of several *E. coli* heat shock proteins has revealed functions that significantly alter this paradigm. We have shown that FtsJ, a well-conserved heat shock protein, is structurally related to methyltransferases and is involved in 23S rRNA methylation in the cell. We have previously described another RNA binding heat shock protein, Hsp15, that binds with high affinity to 50S ribosomal subunits (Korber et al., 2000). Hsp15's crystal structure revealed that it comprises a novel RNA binding motif shared by over 500 sequenced proteins including ribosomal protein S4 and some tRNA synthetases (Staker et al., 2000). Functional analysis suggested that Hsp15 is involved in recycling 50S ribosomal subunits that are blocked by nascent chains. An additional protein involved in RNA metabolism, the tRNA dimethylallyl diphosphate transferase MiaA, is under heat shock regulation (Tsui et al., 1996). The described functions of all of these novel heat shock proteins suggest that protein damage control is clearly not the sole role of the heat shock proteins in the cell. Our results show that RNA-related functions are also important in the heat shock response.

A Different Approach: Structural and Functional Genomics

The classical biochemical approach to identify enzymes has been the fractionation of cell extracts and the purification of enzymes based on activity. This approach is clearly limited to enzymes with rather high specific activity whose substrates are known. The fact that about 30% of all open reading frames, even in well-characterized organisms like *E. coli*, lack any assigned function, suggests that innovative approaches are necessary to complete the characterization of the proteins in model organisms. This problem appears to be particularly acute for methyltransferases, where lack of appropriate substrates, instability, or low activity of the enzymes, as well as possible redundancies of their in vivo functions, have hampered their identification and functional characterization. Fourteen methylations of 23S rRNA are known, but only three 23S rRNA methylating activities in *E. coli* have been described to the level of partial purification (reviewed by Björk, 1996) and only one has been well characterized (Gustafsson and Persson, 1998). Sophisticated sequence comparisons in combination with structural biology now open up the use of very powerful genome-based approaches.

FtsJ was predicted to be an AdoMet-binding protein, suggesting that it functions as a methyltransferase. Structural and functional analysis showed FtsJ to be a novel AdoMet-dependent methyltransferase under heat shock regulation. The 1.5 Å structure of FtsJ revealed a single domain methyltransferase fold and a conserved binding site for the AdoMet cofactor. Immediately noticeable was a distinct cleft adjacent to the AdoMet binding site that is lined with highly conserved, positively charged residues. This could represent the nucleic acid binding site of FtsJ. FtsJ's substrate was found to be folded 23S rRNA that is present within the mature 50S ribosomal subunits. The in vitro ability of FtsJ to recognize and methylate certain tRNAs as well could represent a dual substrate specificity of FtsJ. A detailed comparison of the in vivo methylation pattern of individual isoacceptor tRNAs prepared from *ftsJ* deletion strains and wild-type cells, however, is clearly necessary to answer this question.

Biochemical and genetic techniques were applied to show that FtsJ functions as a 23S rRNA methyltransferase both in vitro and in vivo. Analysis of modification patterns in 23S rRNA prepared from *ftsJ* deletion and wild-type strains showed a clear decrease in 2′O-methyluridine, the nucleoside suggested to be methylated by FtsJ in vitro (Caldas et al., 2000). Furthermore, analysis of polysome profiles prepared from strains deleted for FtsJ indicated that methylation of 23S rRNA plays a very important role in the assembly or stability of ribosomes.

Structure comparisons firmly supported our functional analysis, which suggested that FtsJ acts as 2′O-methyltransferase. The putative substrate binding pocket of FtsJ was found to be structurally similar to the binding pocket of VP39, which also methylates a 2′-hydroxyl of RNA but specifically targets the ribonucleotide immediately following the 5′-(m^7G)ppp-cap of mRNA. The two structures contain a number of identical residues (see above) many of which seem to be involved in substrate binding. These include Lys-175, which in the VP39-RNA hexamer complex structure (Hodel et al., 1998) forms a salt bridge with the RNA phosphate backbone immediately adjacent to the methylated nucleoside. We expect that FtsJ will coordinate its rRNA substrate in a manner analogous to VP39, especially in the area adjacent to AdoMet and the catalytic reaction site. However, we will not expect that FtsJ would mimic VP39's specificity since FtsJ lacks two aromatic side chains of VP39 (*Tyr-22* and *Phe-180*) necessary for binding the 5′-m^7G of mRNA (Hu et al., 1999). How FtsJ recognizes the specific nucleoside(s) surrounding its target nucleoside in 23S rRNA and/or detects the tertiary structure assumed by the 23S RNA in the context of the 50S subunit will necessitate a structure of FtsJ bound to an appropriate oligonucleotide or the 50S ribosome itself. Our studies suggest that the amino-terminal 30 residues not visualized in our structure might fulfill part of this role.

Posttranscriptional Modifications under Heat Shock Control

FtsJ deletion mutants fail to form single colonies on plates, are temperature sensitive, and show a more than 90 min delay before growth resumes following temperature shifts from 30°C to 43°C. This indicated a severe limitation in one or more growth rate–determining factors in *ftsJ* deletion strains. Analysis of polysome profiles of *ftsJ* deletion strains confirmed that translational activity, one of the major growth-determining steps in *E. coli*, is likely to be severely impaired in cells where FtsJ is missing. Accumulation of large amounts of ribosomal subunits in expense of 70S ribosomes and polysomes is characteristic for the polysome profile of *ftsJ* deletion strains. Consistent with this, Spb1, an 841 amino acid essential yeast protein whose N-terminal portion shows significant similarity to *E. coli* FtsJ, was recently implicated in 60S ribosomal subunit biogenesis in *Saccharomyces cerevisiae* (Pintard et al., 2000). This finding sheds new light on the role of posttranscriptional modifications in ribosome assembly and stability. The importance of modified nucleotides in rRNA has long been suggested, since their locations correlate well with universally conserved nucleotides and are known to cluster near the functional center of the ribosome (Brimacombe et al., 1993). Three ribose methylations in *E. coli* 23S rRNA, for example, occur on universally conserved nucleotides within the peptidyltransferase center of the domain V (Gm_{2251}, Cm_{2498}, and Um_{2552}). While modifications in 16S rRNA are not essential for the proper assembly of 30S ribosomal subunits in reconstitution experiments (Krzyzosiak et al., 1987), only in vivo modified 23S rRNA can be used for the in vitro assembly of functional 50S subunits (Green and Noller, 1996). This clearly indicates a requirement of posttranscriptional modifications in the assembly of 50S ribosomal subunits. So far, however, only a few modified nucleotides in rRNAs have been assigned a role in ribosome assembly or peptidyltransferse activity (Green and Noller, 1996). One of these required modifications might be the ribose methylation of U_{2552}, the nucleotide identified to be methylated by FtsJ in vitro (Caldas et al., 2000). Mutations that alter U_{2552} cause severly reduced growth rates (Porse and Garrett, 1995). Furthermore, significant reduction in peptidyltransferase activity has been associated with these mutations, indicating that the presence of Um_{2552} in the A site of the ribosome plays an important role in protein translation (Porse and Garrett, 1995). This is consistent with the finding that the methylated ribose Um_{2791} (corresponding to Um_{2552} in *E. coli* 23S rRNA) is one of only three bases that are modified in the minimally modified 21S rRNA of yeast mitochondria (Sirum-Connolly et al., 1995). YGN6, the most closely related FtsJ homologue from *S. cerevisiae*, is predicted by PSORT to be localized to the mitochondria, suggesting that it might be responsible for Um_{2791} methylation in this compartment as well.

As functions are determined for these novel heat shock proteins, a pattern emerges that connects RNA metabolism with the heat shock response. Of the three heat shock proteins implicated in RNA metabolism, two are now known to be involved in ribosome assembly or stability. Hsp15, a very abundant 23S rRNA binding heat shock protein, appears to be involved in recognition and repair of 50S ribosomal particles that are a product of erroneous dissociation of elongating ribosomes prior to the termination step (Korber et al., 2000). The specific state of 50S ribosomal subunits that is recognized by Hsp15 accumulates during heat shock treatment of the cells. Our work now reveals a surprising connection between rRNA modifications and the heat shock response. It is known that posttranscriptional modifications in tRNA and rRNA are especially abundant in thermophilic organisms, where they are thought to play a functional role in structural stabilization of RNA at elevated temperatures (Noon et al., 1998). For instance,

64%–86% of all modifications in 16S and 23S rRNA of *Sulfolobus solfataricus* have been identified to be ribose methylations at O-2′ and have been shown to further increase with increasing growth temperatures (Noon et al., 1998). Furthermore, ribose methylations such as those mediated by FtsJ appear to enhance local RNA rigidity, increase the T_m, and make the RNA more nuclease resistant (Noon et al., 1998). In the present study, we have provided evidence that the FtsJ-mediated methylation of 23S rRNA is necessary for either the proper assembly of the ribosome or its structural stability once formed. This methylation appears to be necessary under both heat shock and normal growth conditions. Since little is known about the effects of heat treatment on ribosome stability and RNA modification in *E. coli*, additional work is clearly necessary to explore the surprising connection we have made between ribosome biology, RNA methylation, and the heat shock response.

Experimental Procedures

Strains

Strain SK8830 (*ftsJΔ567 thyA715 argG6 zgi-203*::Tn*10*) containing an in-frame deletion in *ftsJ* was constructed using the two-step overlapping PCR procedure described by Ho et al. (1989). The following two pairs of PCR primers were used to amplify a 615 nucleotide DNA fragment from pWSK927 (R.-F. Wang and S. R. Kushner, unpublished results) in which the first six nucleotides of the *ftsJ* coding sequence were fused in-frame to the 30 nucleotides at the carboxyl end: FTSJDEL1-5′-GGTCGCTACAATATACACGCTGGCA GAACGCTTCTTACC-3′; FTSJDEL2-5′-GGTAAGAAGCGTTCTG CCAGCGTGTATATTGTAGCGACC-3′; FTSJPSTI-5′-GATCCTGCAG CGTTTTACCGATGACC-3′; MRSCKPNI-5′-CGTTTTACCGGTACC CGGAGG-3′.

The primers were also designed such that a Pst I site was created at one end of the fragment and a Kpn I site was generated at the other end. After amplification, the DNA fragment was sequenced and subsequently cloned into pMAK705 (Hamilton et al., 1989) to generate pFZK110 (*ftsJΔ567 ori*^{ts} Cm^R). The *ftsJΔ567* allele was recombined into the chromosome of SK5662 (*thyA715 argG6 zgi-203*::Tn*10*) using the gene replacement technique described by Hamilton et al. (1989). Potential *ftsJΔ567* mutants were initially identified by their slow growth phenotype and subsequently confirmed using Southern blot analysis. P1 transduction using the Tc^R of the Tn*10* marker (90% linked to the *ftsJ567* deletion) as the selected marker was used to transfer the *ftsJΔ567* allele into MG1655 generating HB23 (*zgi-203*::Tn*10*, Tc^R, *ftsJΔ567*) and the isogenic WT strain HB24 (*zgi-203*::Tn*10*, Tc^R). Transformation of HB23 with the FtsJ expression plasmid pHB1 resulted in the strain HB25. Western blot experiments indicated that this strain expressed about the same level of FtsJ as the WT strain MG1655. HB30 was constructed by transforming the *hslR* overexpressing plasmid pTHZ25 into HB23 (*ftsJΔ567*) (Table 2).

Sequence Analysis

To find homologs of *E. coli* FtsJ, the NCBI nonredundant database and the incomplete genomes database were searched with a single iteration of PSI-BLAST (Altschul et al., 1997). This yielded a set of 29 likely orthologs, which were aligned with Clustal W. Each ortholog was then used as a seed for an exhaustive iterative search (E-value cutoff = 0.001, 10 cycles maximum, low-complexity regions filtered) against the nonredundant database. The union of these 29 searches yielded 1141 homologs that shared between 4% and 82% sequence identity to *E. coli* FtsJ. Residual redundancies in the database were compensated for by eliminating one of each pair that shared >98% identity. This method is reasonably robust and succeeded in the identification of four out of seven representative structural homologs (as defined by Dali; Holm and Sander, 1993). In addition to many methyltransferases, the sequences of many short-chain oxidoreductases containing the structurally related Rossmann fold were selected. The set of 1112 nonredundant paralogs sequences were aligned to the orthologs using a hidden Markov model (Eddy, 1998) constructed from the ortholog multiple-sequence alignment. Residue conservation was computed from the multiple sequence alignment by a method that allows for conservative (or expected) amino acid substitutions and accounts for sequence weighting effects (E. B. F., unpublished data). Residue conservation was computed separately for just the orthologs and for all the paralogs.

Cloning and Purification of FtsJ

The forward and reverse primers used for amplifying the wild-type *ftsJ* gene from Kohara clone 521 by PCR were 5′-CCATGGGAAAGT CATATGACAGGTAAG-3′ and 5′-CTTTCGTCTGAGATCTCCCGG-3′, respectively. The cloned *ftsJ* open reading frame was ligated into pET11a (pHB1) and transformed into *E. coli* BL21 (DE3). Cells were grown to an OD_{600} of 0.8 at 37°C in LB medium containing 100 μg/ml ampicillin. FtsJ expression was induced with 1 mM IPTG and cells were harvested 4 hr after induction. The cell pellet was resuspended in 40 ml buffer A (40 mM HEPES-KOH, 150 mM KCl [pH 8.0], 2% glycerol, 1 mM DTT, 1 tablet Boehringer Complete protease inhibitor mix) and lysed (French Press, 3 cycles, 14,000 psi). The cleared supernatant was applied onto a tandem Q-Sepharose column followed by a SP-Sepharose column (Pharmacia) equilibrated in buffer A. FtsJ bound exclusively to the SP-Sepharose and eluted around 400 mM KCl in buffer A. FtsJ-containing fractions were loaded onto a Superdex 75 column (Pharmacia) equilibrated in buffer B (40 mM HEPES-KOH, 400 mM KCl, 2% glycerol, 1 mM DTT [pH 7.0]). Highly purified FtsJ fractions were pooled and dialyzed against storage buffer (40 mM HEPES-KOH, 150 mM KCl, 0.6 mM DTT, 2% glycerol [pH 7.0]). The purity of FtsJ was estimated to be >98%. For concentration determination, the extinction coefficient of 1.0 for a 1 mg/ml solution at A_{280} was used (Gill and von Hippel, 1989).

Structure Determination

Crystals of FtsJ were grown by mixing 2 μl of FtsJ (12 mg/ml FtsJ in storage buffer) with 1 μl 1 mM AdoMet and 2 μl of precipitant (33% PEG 4000, 0.19 M ammonium acetate, 0.1 M sodium citrate [pH 5.7]). The drop was equilibrated against 1 ml of the same precipitant by microvapor diffusion. Only four large crystals were obtained. Prior to data collection, crystals were soaked in a cryoprotectant of 15% glycerol in precipitant. Heavy atom soaks were performed in the same solution.

Data were collected on a Rigaku R-AXIS IV/RU-H3R detector system operating at 50 kV, 100 mA. Intensities were integrated, scaled, and merged with HKL (Otwinowski and Minor, 1997) and converted to amplitudes by the method of French and Wilson (1978). Crystals were of space group $P2_12_12_1$ with a = 36.46 Å, b = 65.87 Å, c = 72.88 Å. The native crystal diffracted to at least 1.5 Å. With only three crystals remaining, heavy atom derivatives were carefully selected based on success in previous methyltransferase structure determinations. Crystals soaked in $HgCl_2$, K_2PtCl_4, and uranyl acetate were used as derivatives. Sites for each derivative were found by Patterson techniques, and confirmed in difference Fourier maps. Heavy atom sites were refined and phases were calculated to 1.5 Å with MLPHARE (Collaborative Computational Project No. 4, 1994). The overall figure of merit was 0.47, which increased to 0.63 after solvent flattening with DM.

With the C_α trace of catechol O-methyltransferase (PDB entry 1VID; Vidgren et al., 1994) as a guide and the excellent 1.5 Å MIRAS electron density maps, the FtsJ chain was quickly traced and side chains modeled with O (Jones et al., 1991). The model was refined using CNS (Brünger et al., 1998) to only 1.7 Å because of poor completeness in the 1.5–1.7 Å shell of the native data set. A bulk solvent correction was applied. The final model contains 180 residues (30–209), 183 water molecules, and 1 AdoMet, with R_{cryst} = 0.191 and R_{free} = 0.238. The rmsd from ideality was 0.013 Å for bonds and 1.7° for angles. The model was also refined against the mercury derivative data to a resolution of 1.5 Å with R_{cryst} = 0.182, R_{free} = 0.218, rmsd of bonds = 0.017 Å, and rmsd of angles = 1.87°. The rmsd between native and mercury-containing structures was 0.23 Å for C_α atoms and 0.6 Å for all atoms.

Preparation and Purification of RNA Transcripts

In vitro transcriptions of 16S, 23S rRNA, and *hslR* were performed using the MEGAscript T7 in vitro transcription kit (Ambion) according

to the manufacturer's protocol. The RNA transcripts were purified using the RNeasy RNA kit (Qiagen) according to the manufacturer's protocol. RNA concentrations were determined using an extinction of 1.0 (A_{260}) for a 40 μg/ml solution. Unmodified *B. subtilis* $tRNA^{Asp}$ was a kind gift of David Engelke (University of Michigan).

Polysome Profiles and Preparation of Ribosomal Subunits

Lysates of strains HB23 and HB24 were prepared as previously described (Korber et al., 2000) in the presence of 80 U RNaseIn (Promega). Analytical polysome profiles were obtained by ultracentrifugation (Beckman L8-70 centrifuge with SW40 Ti rotor) of the lysates (A_{260} = 2 U) in 10%–50% sucrose gradients (2°C, $\omega^2 t = 2.87 \times 10^{11}$ rad^2/s) under the salt conditions indicated in the figure legends. The sucrose gradients were analyzed as described (Korber et al., 2000).

Ribosomal subunits were prepared by ultracentrifugation of the lysates (A_{260} = 20 U) on either 10%–50% (Figure 5B) or 5%–25% (Figure 7B) sucrose gradients under nonstringent conditions (1 mM $MgCl_2$, 200 mM NH_4Cl). Fractions containing ribosomal subunits were collected, and the sucrose was removed using a PD10 (Amersham) gel filtration column equilibrated in 6-30 buffer (20 mM HEPES-KOH, 6 mM $MgCl_2$, 30 mM NH_4Cl, 4 mM β-mercaptoethanol [pH 7.5]). The ribosomal subunits were pelleted (20 hr, 190,000 × g, 4°C), resuspended in 6-30 buffer, and the subunit concentration was determined according to Bommer et al. (1996).

Methyltransferase Assay

FtsJ's methyltransferase activity was monitored using a modification of the assay described by Tscherne et al. (1999). FtsJ (0.5 μM) was incubated with 50 μM of ^{3}H-methyl AdoMet (80 μCi/ml; Amersham) in methylation buffer (50 mM Tris-HCl [pH 7.5], 100 mM NH_4Cl, 3-4.2 mM $MgCl_2$, 0.1 mg/ml BSA, 1 mM DTT), and the methylation reaction was started by the addition of the various RNA transcripts (2 μM) or 50S subunits of WT and *ftsJ* deletion strain, respectively. At the time points indicated, 6 μl aliquots were taken, and the reaction was terminated by immediate precipitation with ice-cold trichloracetic acid (5% final concentration). Carrier tRNA (40 μg) was added to the vitro transcripts prior to TCA precipitation. For detailed methylation analysis of the individual particles (Figure 7B), fractions were pooled and concentrated as described above. Methylation reactions were performed using 0.1 μM FtsJ, 2 μM subunits, and 8 μM ^{3}H-methyl AdoMet (320 μCi/ml) in 50 mM Tris-HCl [pH 7.5], 100 mM NH_4Cl, 4.2 mM $MgCl_2$. Reactions were terminated after 150 min incubation at 37°C by immediate precipitation with ice-cold trichloracetic acid (5% final concentration). After 15 min of incubation on ice, the RNA precipitates were pelleted by centrifugation (13,000 rpm, 15 min, 4°C), washed with 500 μl 5% TCA, dissolved in 50 μl 0.1 M Tris-HCl (pH 8.0), and TCA precipitated a second time. Acid-insoluble material was collected on nitrocellulose filters (Millipore), washed with 10 ml 5% TCA, air dried, and counted in a Beckman LS 6800 Liquid Scintillation counter.

Dot Blots

Linearized plasmids carrying the genes for 16S rRNA and 23S rRNA were used as probes and labeled with the nonisotopic BrightStar Psoralen-Biotin labeling kit (Ambion) according to the manufacturer's protocol. Polysome profiles of HB23 and HB24 lysates were fractionated as described, and aliquots of each fraction were incubated at 65°C for 5 min in a final concentration of 2.2 M formaldehyde, 50% (v/v) formamide, 10 mM MOPS, 4 mM NaCl, 0.5 mM EDTA (pH 7.0) and cooled in ice water. Prior to spotting onto a prewetted Hybond N^+ membrane (Amersham), the samples were adjusted to a final concentration of 10× SSC buffer. Two microliters aliquots were spotted. Hybridization was performed overnight at 68°C according to the membrane manufacturer's protocol. Washing and detection were performed using the BrightStar BioDetect Detection Kit (Ambion) according to the manufacturer's protocol.

Acknowledgments

We thank Dr. James McCloskey and Dr. Fenge Qiu for determining the modification pattern of tRNAs and 23S rRNAs. Many thanks to Dr. Philipp Korber for numerous suggestions, to Rebecca Schutt for crystal growth expertise, to Jaqueline Tan for phenotypical studies, and to Stacie Novakovic for excellent technical assistance. We thank Drs. David Engelke, George Garcia, Rachel Green, Kate Noon, and Rainer Jaenicke for many helpful discussions. This work was supported by a DAAD doctoral fellowship to H. B., a NIH Genetics Training Grant to B. L. S., and NIH grants to J. C. A. B. and M. A. S. J. C. A. B. is a Pew Scholar in the Biomedical Sciences.

Received March 10, 2000; revised June 15, 2000.

References

Altschul, S.F., Madden, T.L., Schaffer, A.A., Zhang, J., Zhang, Z., Miller, W., and Lipman, D.J. (1997). Gapped BLAST and PSI-BLAST: a new generation of protein database search programs. Nucleic Acids Res. *25*, 3389–3402.

Becker, J., and Craig, E.A. (1994). Heat-shock proteins as molecular chaperones. Eur. J. Biochem. *219*, 11–23.

Björk, G.R. (1996). In *E. coli* and Salmonella Cellular and Molecular Biology, F.C. Neidhardt, ed. (Washington, D.C.: ASM Press) 2nd edition, pp. 861–880.

Bussiere, D.E., Muchmore, S.W., Dealwis, C.G., Schluckebier, G., Nienaber, V.L., Edalji, R.P., Walter, K.A., Ladror, U.S., Holzman, T.F., and Abad-Zapatero, C. (1998). Crystal structure of ErmC', an rRNA methyltransferase which mediates antibiotic resistance in bacteria. Biochemistry *37*, 7103–7112.

Brimacombe, R., Mitchell, P., Osswald, M., Stade, K., and Bochkariov D. (1993). Clustering of modified nucleotides at the functional center of bacterial ribosomal RNA. FASEB J. *7*, 161–167.

Brünger, A.T., Adams, P.D., Clore, G.M., DeLano, W.L., Gros, P., Grosse-Kunstleve, R.W., Jiang, J.-S., Kuszewski, J., Nilges, N., Pannu, N.S., et al. (1998). Crystallography and NMR system (CNS): a new software system for macromolecular structure determination. Acta Crystallogr. D Biol. Crystallogr. *54*, 905–921.

Caldas, T., Binet, E., Bouloc, P., Costa, A., Desgres, J., and Richarme, G. (2000). The FtsJ/RrmJ heat shock protein of *Escherichia coli* is a 23S ribosomal RNA methyltransferase. J. Biol. Chem. *275*, 16414–16419.

Carson, M. (1997). Ribbons. In Methods in Enzymology, R.M. Sweet and C.W. Carter, eds. (New York: Academic Press), pp. 493–505.

Collaborative Computational Project, Number 4 (1994). The CCP4 suite: programs for protein crystallography. Acta. Crystallogr. D Biol. Crystallog. *50*, 760–763.

Djordjevic, S., and Stock, A.M. (1997). Crystal structure of the chemotaxis receptor methyltransferase CheR suggests a conserved structural motif for binding S-adenosylmethionine. Structure *5*, 545–558.

Eddy, S.R. (1998). Profile hidden Markov models. Bioinformatics *14*, 755–763.

Fauman, E.B., Blumenthal, R.M., and Cheng, X. (1999). Structure and evolution of AdoMet-dependent methyltransferases. In S-Adenosylmethionine-Dependent-Methyltrans-ferases: Structures and Functions, X. Cheng, and R.M. Blumenthal, eds. (River Edge, N.J.: World Scientific), pp. 1–38.

French, G.S., and Wilson, K.S. (1978). On the treatment of negative intensity observations. Acta Crystallogr. A *34*, 517–525.

Gill, S.C., and von Hippel, P.H. (1989). Calculation of protein extinction coefficients from amino acid sequence data. Anal. Biochem. *182*, 319–326.

Green, R., and Noller, H.F. (1996). In vitro complementation analysis localizes 23S rRNA posttranscriptional modifications that are required for *Escherichia coli* 50S ribosomal subunit assembly and function. RNA *2*, 1011–1021.

Gross, C.A. (1996). In *E. coli* and Salmonella Cellular and Molecular Biology. F.C. Neidhardt, ed. (Washington, D.C.: ASM Press), 2nd edition, pp. 1382–1399.

Gustafsson, C., and Persson, B.C. (1998). Identification of the rrmA gene encoding the 23S rRNA m1G745 methyltransferase in *Escherichia coli* and characterization of an m1G745-deficient mutant. J. Bacteriol. *180*, 359–365.

Hamilton, C.M., Aldea, M., Washburn, B.K., Babitzke, P., and Kushner, S.R. (1989). A new method for generating deletions and gene replacements in *Escherichia coli*. J. Bacteriol. *171*, 4617–4622.

Ho, S.N., Hunt, H.D., Horton, R.M., Pullen, J.K., and Pease, L.R. (1989). Site-directed mutagenesis by overlap extension using the polymerase chain reaction. Gene *77*, 51–59.

Hodel, A.E., Gershon, P.D., Shi, X., and Quiocho, F.A. (1996). The 1.85 Å structure of vaccinia protein VP39: a bifunctional enzyme which participates in the modification of both mRNA ends. Cell *85*, 247–256.

Hodel, A.E., Gershon, P.D., and Quiocho, F.A. (1998). Structural basis for sequence-nonspecific recognition of 5′-capped mRNA by a cap-modifying enzyme. Mol. Cell *1*, 443–447.

Holm, L. and Sander, C. (1993). Protein structure comparison by alignment of distance matrices. J. Mol. Biol. *233*, 123–128.

Hu, G., Gershon, P.D., Hodel, A.E., and Quiocho, F.A. (1999). mRNA cap recognition: dominant role of enhanced stacking interactions between methylated bases and protein aromatic side chains. Proc. Nat. Acad. Sci. US*A 96*, 7149–7154.

Jones, T.A., Zou, J.-Y., Cowan, S.W., and Kjeldgaard, M. (1991). Improved methods for building protein models in electron density maps and the location of errors in these models. Acta Crystallogr. A *47*, 110–119.

Kleywegt, G.J., and Jones, T.A. (1997). Detecting folding motifs and similarities in protein structures. Meth. Enzymol. *277*, 525–545.

Koonin, E.V. (1994). Prediction of an rRNA methyltransferase domain in human tumor-specific nucleolar protein P120. Nucleic Acids Res. *22*, 2476–2478.

Korber, P., Stahl, J.M., Nierhaus, K.H., and Bardwell, J.C.A. (2000). Hsp15: a ribosome-associated heat shock protein. EMBO J. *19*, 741–748.

Krzyzosiak, W., Denman, R., Nurse, K., Hellmann, W., Boublik, M., Gehrke, C.W., Agris, P.F., Ofengand, J. (1987). In vitro synthesis of 16S ribosomal RNA containing single base changes and assembly into a functional 30S ribosome. Biochemistry *26*, 2353–2364.

Nichols, A., Sharp, K.A., and Honig, B. (1991). Protein folding and association: insights from the interfacial and thermodynamic properties of hydrocarbons. Proteins *11*, 281–296.

Noon, K.R., Bruenger, E., and McCloskey, J.A. (1998). Posttranscriptional modifications in 16S and 23S rRNAs of the archaeal hyperthermophile Sulfolobus solfataricus. J. Bacteriol. *180*, 2883–2888.

Ogura, T., Tomoyasu, T., Yuki, T., Morimura, S., Begg, K.J., Donachie, W.D., Mori, H., Niki, H., and Hiraga, S. (1991). Structure and function of the *ftsH* gene in *Escherichia coli*. Res. Microbiol. *142*, 279–282.

Otwinowski, Z., and Minor, W. (1997). Processing of X-ray diffraction data collected in oscillation mode. Meth. Enzymol. *276*, 307–326.

Pintard, L., Kressler, D., and Lapeyrek, B. (2000). Spb1p is a yeast nucleolar protein associated with Nop1p and Nop58p that is able to bind S-adenosyl-L-methionine in vitro. Mol. Cell Biol. *20*, 1370–1381.

Porse, B.T., and Garrett, R.A. (1995). Mapping important nucleotides in the peptidyl transferase center of 23 S rRNA using a random mutagenesis approach. J. Mol. Biol. *249*, 1–10.

Richmond, C.S., Glasner, J.D., Mau, R., Jin, H., and Blattner, F.R. (1999). Genome wide expression profiling in *Escherichia coli* K-12. Nucleic Acids Res. *27*, 3821–3835.

Schluckebier, G., Kozak, M., Bleimling, N., Weinhold, E., and Saenger, W. (1997). Differential binding of S-adenosylmethionine S-adenosylhomocysteine and Sinefungin to the adenine-specific DNA methyltransferase M. TaqI. J. Mol. Biol. *265*, 56–67.

Sirum-Connolly, K., Peltier, J.M., Crain, P.F., McCloskey, J.A. and Mason, T.L. (1995). Implications of a functional large ribosomal RNA with only three modified nucleotides. Biochimie *77*, 30–39.

Staker, B., Korber, P., Bardwell, J.C.A. and Saper, M.A. (2000). Structure of Hsp15 reveals a novel RNA-binding motif. EMBO J. *19*, 749–757.

Tscherne, J.S., Nurse, K., Popienick, P., Michel, H., Sochacki, M., and Ofengand, J. (1999). Purification, cloning, and characterization of the 16S RNA m^5C967 methyltransferase from *Escherichia coli*. Biochemistry *38*, 1884–1892.

Tsui, H.C., Feng, G., and Winkler, M.E. (1996). Transcription of the *mutL* repair, *miaA* tRNA modification, *hfq* pleiotropic regulator, and *hflA* region protease genes of *Escherichia coli* K-12 from clustered sigma32-specific promoters during heat shock. J. Bacteriol. *178*, 5719–5731.

Vidgren, J., Svensson, L.A., and Liljas, A. (1994). Crystal structure of catechol O-methyltransferase. Nature *368*, 354–358.

Wallace, A.C., Laskowski, R.A., and Thornton, J.M. (1995). LIGPLOT: a program to generate schematic diagrams of protein-ligand interactions. Protein Eng. *8*, 127–134.

Protein Data Bank ID Codes

Coordinates for the native and mercury derivative structures were submitted to the Protein Data Bank with entry codes 1EIZ and 1EJ0, respectively.